Journal of Environmental Chemical Engineering 11 (2023) 110200

Contents lists available at ScienceDirect

Journal of Environmental Chemical Engineering

journal homepage: www.elsevier.com/locate/jece

Effect of interaction degree between Mn and Ce of MnO_X-CeO_2 formulation on NO reduction and o-DCB oxidation performed simultaneously

J.A. Martín-Martín, M.P. González-Marcos, A. Aranzabal *, J.R. González-Velasco

Group of Chemical Technologies for Environmental Sustainability, Departmentof Chemical Engineering, Faculty of Science and Technology, The University of the Basque Country, UPV/EHU, P.O. Box 644, E-48080 Bilbao, Spain

ARTICLE INFO

Editor: Fumitake Takahashi

Keywords:
MnO_X-CeO_2
Preparation method
NO reduction
O-DCB oxidation
Mn and Ce interaction

ABSTRACT

MnO_X-CeO_2 catalysts were prepared by different methods in order to assess the influence of Mn and Ce interaction on the catalytic activity of NO reduction and 1,2-dichlorobencene (o-DCB) oxidation carried out simultaneously. Changes on catalytic properties were evaluated by XRD, Raman, N_2-physisorption, H_2-TPR and NH_3-TPD. The samples prepared by co-precipitation and sol-gel exhibited the best catalytic activity over the whole temperature range. These preparation methods provide high interaction between Mn and Ce at surface and bulk, which was evidenced by the formation of mixed oxide phase. According to characterisation, the enhancement of catalytic activity with Mn and Ce interaction is associated to the promotion of structural defects, which improve redox and acid properties. Oxidative capability is also improved as a consequence of the oxygen vacancies generated by the presence of those structural defects. On the other hand, the promotion of Mn and Ce interaction favours the production of N_2O in NO reduction at a lower temperature, and also leads to o-DCB total oxidation by decreasing CO production.

1. Introduction

Current waste management regulations establish a hierarchy in which any way of recovery is encouraged before disposal [1]. In this context, municipal solid waste incineration is promoted over landfilling because it allows the possibility of recovering the energy released in the combustion of waste to produce heat and/or electricity. However, incineration processes generate a wide variety of pollutants among which NO_X and PCDD/Fs are some of the most harmful to the environment and living beings.

In incineration plants, NO_X are removed from the combustion exhaust gases by selective reduction with ammonia precursor compounds, such as urea, ammonium hydroxide, etc. There are two processes: the non-catalytic reduction, that occurs by adding the reducing agent into the furnace; and the catalytic reduction, that requires a specific catalytic unit for this purpose. Selective catalytic reduction (SCR) features higher efficiency and reducing agent savings [2,3], hence it is promoted in the light of the expected tightening of emission limits in the future. On the other hand, PCDD/Fs are usually removed by adsorption processes which allow to meet the emission limits, but have the disadvantage of not destroying the pollutant (which is only moved from the gas phase to the adsorbent) and generate a waste that needs to be treated [4,5].

The conventional catalyst for SCR in stationary sources is based on V oxide as the active phase and promoted with W and/or Mo oxide [2]. This catalytic formulation has also been reported to be active in the removal, by catalytic oxidation, of PCDD/Fs both at full and pilot scale [6–8]. This ability of the SCR catalyst brings the possibility of abating simultaneously two different pollutants, such as NO_X and PCDD/Fs (and/or chlorinated organic compounds) in a single stage. In fact, this process has already been considered in the Best Available Technique Reference Document for Waste Incineration by the Join Research Centre, European Commission's in-house science service [9].

Currently, in order to perform the SCR at lower temperatures, some alternative formulations to the conventional SCR catalyst are under investigation. These alternative catalytic formulations mainly study Mn and Fe oxides as active components [10–13] and their combination with other transition metals, such as Cu [14], Ce [15–17], Co [18,19], etc., whose interactions with the active metal can improve the catalytic performance. Moreover, exchanged zeolites with Fe and Cu are also considered, because of their good catalytic performance in the high temperature range [10,20]. Among them, MnO_X-based catalysts are

* Corresponding author.
E-mail address: asier.aranzabal@ehu.eus (A. Aranzabal).

https://doi.org/10.1016/j.jece.2023.110200
Received 22 December 2022; Received in revised form 27 April 2023; Accepted 24 May 2023
Available online 25 May 2023

extensively studied due to their high catalytic activity for low temperature SCR, especially those doped with Ce. Ce-doping improves oxygen storage and mobility along the catalytic structure at both surface and bulk, which favors redox and acid properties. Hence, Mn and Ce composite oxides are reported to reach full NO conversion between 100 and 200ºC [15,17,21].

Mn and Ce composite oxides are also reported to be highly active for oxidation reactions, which means that NO_X and PCDD/Fs can also be abated simultaneously. However, the majority of works in the literature focus on the study of catalytic oxidation activity with model compounds of PCDD/Fs and in the absence of NO_X. In this regard, Liu and co-workers reported total conversion in o-DCB oxidation with MnO_X as the active phase supported over several materials [22]. Catalytic activity of Mn-based catalysts is improved by doping with one to several transition metals, such as Cu, Ti and Co [23–25]. Nonetheless, Mn doped with Ce is the most referenced formulation and it has been extensively studied in the catalytic oxidation of different VOCs [26,27], such as hexane, toluene, etc.; and chlorinated organic compounds, such as chlorinated benzene and trichloroethylene [28,29]. Moreover, Martín-Martín and co-workers [30] studied the feasibility of MnO_X-CeO_2 formulation in the simultaneous removal of NO and o-DCB and corroborated that catalysts with high Mn contents allow high conversion of both pollutants in the same temperature range, between 200 and 250 ºC.

Therefore, Mn and Ce composite oxides are considered to be active in both low temperature SCR and catalytic oxidation reactions. Nonetheless, the interaction between active metals is well known to play a key role in catalytic formulations based on composite oxides because it affects their structural and morphological properties, which define reducibility and acidity. In this sense, the preparation method is reported to be one of the variables most strongly affecting the interaction between active metals: it can promote surface and/or bulk interaction, and even the formation of a mixed oxide phase by the incorporation of one of the active metals to the structure of the other. According to the literature, several preparation methods have been studied for the synthesis of Mn and Ce composite oxides, such as impregnation [31], redox precipitation [21], sol-gel [16]. Nonetheless, there is no agreement on which is the most appropriate to perform SCR and catalytic oxidation reactions.

The main goal of this work is to evaluate several preparation methods for MnO_X-CeO_2 catalytic formulation in order to assess the influence of Mn and Ce interaction on the catalytic activity of NO reduction and o-DCB oxidation carried out simultaneously.

2. Experimental

2.1. Catalyst preparation

Mn and Ce composite oxides were synthetized by several preparation methods, which were selected because they provide different degrees of interaction between Mn and Ce in the resulting samples, as well as they are simple, reproducible and easy to scale. Pure cerium oxide and pure manganese oxide were also prepared.

Pure oxides were prepared by precipitation and using $Mn(NO_3)_2{\cdot}4\ H_2O$ or $Ce(NO_3)_3{\cdot}6\ H_2O$ as precursors. In this procedure, the proper amount of the precursor compounds was solved in distilled water at room temperature, obtaining precursor solutions of Mn or Ce around 0.55 and 0.35 M, respectively. Subsequently, the precipitations of metal cations were carried out by dropwise addition of a 1.3 M solution of ammonium carbamate ($H_2NCOONH_4$), until a pH value of 9 was reached. The resulting suspensions were aged for 2 h and, subsequently, filtered and washed with distilled water.

For the preparation of Mn and Ce composite oxides, four preparation methods were used: mechanical mixing, impregnation, co-precipitation and sol-gel. Mn and Ce contents were selected with the intention to obtain a similar concentration of both metals at the catalytic surface. In this way, an equimolar concentration of Mn and Ce was selected for all bimetallic samples, except for that prepared by impregnation in which a 2% Mn (wt%) was used (the one corresponding to the theoretical half monolayer coverage of the CeO_2 surface). Next, the experimental procedures for each preparation method are detailed:

2.1.1. Mechanical mixing

This method consisted of the physical mixing of pure manganese and cerium oxides after being calcinated and sieved.

2.1.2. Impregnation

The preparation was carried out in a rotary evaporator. Firstly, the proper amount of support (CeO_2, resulting from direct calcination of Ce $(NO_3)_3{\cdot}6\ H_2O$ at 550 ºC for 3 h) was pre-treated in vacuum conditions at 40 ºC for 1 h. Secondly, a solution with the proper amount of Mn precursor was poured to the support. The resulting slurry was homogeneously stirred for 1 h, then, the temperature was increased up to 40 ºC to favour the complete evaporation of the solvent.

2.1.3. Co-precipitation

The procedure is similar to that described above for pure oxides, the only difference being that the precursor solution, to which the precipitating agent is added, contains both Mn and Ce precursors.

2.1.4. Sol-gel

In this method, the appropriate amount of Mn and Ce precursors was solved in distilled water at room temperature. Citric acid, to a molar concentration equal to 0.3(Mn+Ce), was also added as chelating agent. Subsequently, the solution temperature was progressively increased to 80 ºC under continuous stirring, to evaporate the solvent and lead to the formation of the gel.

Finally, the resulting solid from each preparation method was dried over night at 110 ºC and calcined at 500 ºC for 3 h with a heating ramp of 1 ºC/min in static air. Then, the catalyst was sieved to 0.3–0.5 mm.

2.2. Catalyst characterization

The different crystal phases of the catalysts were identified by X-ray diffraction (XRD). The analysis was carried out on a Philips PW 1710 X-ray diffractometer with Cu Kα radiation ($\lambda = 1.5406$ Å) and Ni filter. Each measurement was ranged between 20 and 60º (2θ) with step size of 0.026º and counting time of 528 s. Identification of the crystal phases was made by comparing with JCPDS database cards.

Raman spectroscopy analysis was performed in a Renishaw System 1000 Raman spectrometer with a 706 nm solid-state laser used as excitation line, dosing a power on the sample of 1 mW. Each measurement was performed at room temperature with 20 s per scan and 5 accumulated scans.

N_2 adsorption-desorption isotherms at –196 ºC were used to evaluate textural properties of the samples. The measurements were carried out on a Micromeritics TRISTAR II 3020. Before each analysis, the samples were pre-treated at 350 ºC for 4 h with a flow of N_2. Specific surface area was calculated according to BET procedure, using the data obtained from the adsorption isotherm branch in the relative pressure between 0.03 and 0.3. On the other hand, BJH method was used to estimate pore average size and distribution, using the data from the desorption isotherm branch.

Redox properties of the catalysts were assessed by temperature programmed reduction with H_2 (H_2-TPR). A Micromeritics AutoChem 2920 instrument was used to carry out these experiments. Firstly, the samples (15–20 mg) were pre-treated at 500 ºC for 45 min with 50 cm^3/min of 5% O_2/He mixture and, then, cooled down to 100 ºC in helium. After that, the samples were heated from 100 to 900 ºC at 10 ºC/min under 50 cm^3/min of 5% H_2/Ar. H_2 consumption in the experiment was recorded with a TDC. In order to avoid interferences between water produced and the TCD measurement, water was trapped in a cold trap.

Time integration of TCD signal allowed to calculate the total H_2 consumed.

Temperature programmed desorption of ammonia (NH_3-TPD) was used to study the acidity of the catalysts. A Micromeritics AutoChem 2920 instrument was used to carry out the NH_3-TPD experiments. All samples (15–20 mg) were pre-treated at 500 ºC for 45 min with 50 cm^3/min of 5% O_2/He mixture and, then, cooled down to 50 ºC in helium. The adsorption step of ammonia was performed by feeding 130 cm^3/min of 1% NH_3/He mixture gas at 50 ºC during 60 min. Ammonia weakly adsorbed on the surface of the samples was removed with helium (130 cm^3/min for 60 min). Finally, ammonia desorption was performed by heating the sample from 50 to 500 ºC (10 ºC/min) and using helium as a carrier. A TCD was used to record the NH_3 desorbed, and the total acidity was calculated by time-integration of TCD signal.

2.3. Reaction set-up and catalytic tests

The experimental reaction set-up allows to prepare a gas feeding stream with similar components and concentrations to those found at the inlet of a SCR unit with tail-end configuration at an incineration plant. The flows of gaseous and liquid reagents are regulated by mass flow controllers (Bronkhorst® High-Tech F-201CV and Bronkhorst® High-Tech μ-Flow L01-AAA-99–0–20S, respectively). The complete evaporation of liquid components in the system is ensured by a controlled-evaporator-mixed (Bronkhorst® High-Tech W-102A-111-K), which favors a homogenous mixture with the gas stream as well. All pipes in the experimental set-up are heated with electrical resistances to avoid gas adsorption and condensation.

For the catalytic activity tests, the feeding stream was composed by NO (300 ppm), NH_3 (300 ppm), O_2 (10%), o-DCB (100 ppm) and Ar to balance. It is important to remark that o-DCB was used as model compound PCDD/Fs because of the high toxicity and operational problems that involves working with PCDD/Fs at lab level. Moreover, although CO and CO_2 are components of the gas feeding stream at full scale, they were not considered in this work because we have already checked their presences do not affect the reactions under study and makes it difficult to analyze the selectivity of the oxidation reaction.

On the other hand, the catalytic bed is located inside a tubular U-shape quartz reactor, which is in turn placed inside a convective flow oven. The catalytic bed is composed of 1.5 g of catalyst with 0.3–0.5 mm size diluted in inert quartz until filling a bed volume of 3 cm^{-3}. Before each experiment, the catalytic bed was pre-treated at 200 ºC with a flow of 2 L_N/min of pure Ar for 2 h in order to clean the catalytic surface. The catalytic activity has been evaluated by light-off experiments with a feeding stream of 2 L_N/min (GHSV 40,000 h^{-1}) at a pressure of 1.5 atm and increasing reaction temperature from 100 to 450 ºC with a heating ramp of 1.5 ºC/min.

For the analysis of reaction reagents and products, several analyzers were used: an ABB Limas 21 to continuously measure the concentration of NO, NO_2 and NH_3; an ABB Uras 26 Infrared analyzer to continuously measure the concentration of N_2O, CO and CO_2; and, finally, a gas chromatograph (Agilent Technologies 7890 A) coupled to a mass selective detector (Agilent Technologies 5975 C) to quantify o-DCB concentration and the chlorinated organic by-products of o-DCB oxidation. NH_3 concentration could not be quantified as a consequence of o-DCB interference in ABB Limas 21.

NO and o-DCB conversion was calculated from Eqs. 1 and 2, respectively. Selectivity to CO_2 and CO was calculated through Eqs. 3 and 4, respectively.

$$X_{NO} = \frac{C_{NO,in} - C_{NO,out}}{C_{NO,in}} \cdot 100 \quad (1)$$

$$X_{oDCB} = \frac{C_{o-DCB,in} - C_{o-DCB,out}}{C_{o-DCB,in}} \cdot 100 \quad 2)$$

$$S_{CO_2} = \frac{C_{co_2,out}}{6 \cdot C_{o-DCB,in} - C_{o-DCB,out}} \cdot 100 \quad (3)$$

$$S_{CO} = \frac{C_{co,out}}{6 \cdot \left(C_{o-DCB,in} - C_{o-DCB,out}\right)} \cdot 100 \quad (4)$$

3. Results and discussion

3.1. Catalyst characterization

The influence of preparation method on catalytic structural properties has been firstly studied by XRD. Fig. 1 shows the diffraction patterns of the composite oxides prepared by the studied preparation methods, and two additional ones corresponding to pure cerium and manganese oxides. Pure cerium oxide exhibits diffraction peaks associated to fluorite cubic structure, whereas the diffraction peaks of pure manganese oxide are associated to α-Mn_2O_3 crystal phase.

The sample prepared by mechanical mixing shows diffraction peaks of both fluorite and α-Mn_2O_3, as a consequence of the physical mixing of these pure oxides. However, the diffraction patterns of the samples prepared by impregnation, co-precipitation and sol-gel indicate the majority presence of fluorite phase, which is characteristic of pure cerium oxide. The absence of manganese oxide diffraction peaks in the sample prepared by impregnation is associated to its low Mn content. In the case of the samples prepared by co-precipitation and sol-gel, this fact is associated to Mn incorporation to fluorite structure forming a mixed oxide phase or solid solution [30,32,33], as denotes the broaden of fluorite diffraction peaks and the slight shift to higher Bragg angles of the strongest peak of this crystal phase with respect to pure cerium oxide, clearly noticeable in the inset graph of Fig. 1. Nonetheless, the sample prepared by co-precipitation also shows some very weak peaks around 33 and 38º, which suggests that a very small part of Mn has segregated as Mn_2O_3.

In order to evaluate the structural distortion caused by the formation of the mixed oxide phase, the lattice parameter of fluorite phase was estimated and is reported in Table 1. The values for catalysts prepared by co-precipitation and sol-gel are smaller than that for pure cerium oxide. This result is associated to the contraction of fluorite structure as a consequence of the smaller ionic radius of Mn ions with respect to Ce ions [28], hence it corroborates the formation of a mixed oxide phase.

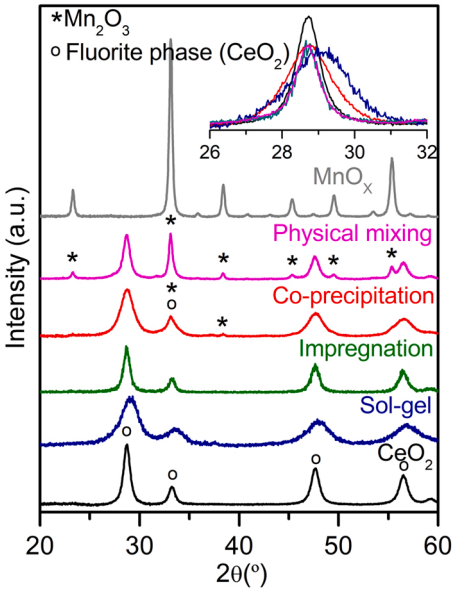

Fig. 1. XRD patterns of MnO_X-CeO_2 samples prepared by different preparation methods. Inset figure: zoom of 2Θ region between 26 and 32º.

Table 1
Structural and textural properties of MnO_X-CeO_2 samples prepared by different methods.

Sample	Fluorite lattice parameter (nm)	Fluorite crystal size (nm)	F_{2g} position (cm^{-1})	FWHM of F_{2g} (cm^{-1})	S_{BET} (m^2/g)	V_p (cm^3/g)
CeO_2	5.4135	9	462	19	80	0.12
Sol-gel	5.3854	3	457	56	63	0.16
Impregnation	5.4161	8	460	23	63	0.17
Co-precipitation	5.4035	4	456	41	88	0.21
Mechanical mixing	5.4117	10	462	20	67	0.14
MnO_X	–	–	–	–	34	0.19

On the contrary, the lattice parameter for the catalysts prepared by mechanical mixing and impregnation is close to that of pure cerium oxide, which means that the amount of Mn incorporated to CeO_2 structure is very low or practically null.

Moreover, Table 1 reports the crystal size of fluorite phase, which was estimated by applying Scherrer equation to the most intense peak of this crystal phase, that is, the one located at 28.6°. The samples prepared by mechanical mixing and impregnation exhibit a crystal size similar to that of pure cerium oxide, whereas the samples prepared by co-precipitation and sol-gel show a lower value. This result is in accordance with the trend in lattice parameter explained above, and is associated to structural defects generated by Mn incorporation to the fluorite structure, which has a negative effect on the growth of fluorite crystal domains of cerium oxide.

Structural properties of the catalysts were also characterized by Raman spectroscopy. The spectra of the samples prepared by different methods and the two pure oxides are shown in Fig. 2. Raman spectrum of pure cerium oxide has an intense peak at 460 cm^{-1} related to F_{2g} mode of CeO_2 [34]. On the other hand, pure manganese oxide exhibits several peaks at 693, 640 and 306 cm^{-1} corresponding to ν_7, ν_6 and ν_2 vibrational modes of α-Mn_2O_3 (in agreement with XRD, where this manganese oxide phase was the only one identified) [35].

The F_{2g} band is common in all Raman spectra of the catalysts prepared by different methods, although, interestingly, its location slightly changes depending on the samples (Table 1). The position in the sample prepared by mechanical mixing is the same as that of pure cerium oxide, whereas it is shifted to lower wavenumbers in all the other bimetallic samples, although this shift becomes larger in those prepared by co-precipitation and sol-gel. F_{2g} band corresponds to the atoms belonging to the structure around Ce^{4+} and their symmetrical stretching vibration [36]. Thus, the displacement just discussed above evidences an alteration in the CeO_2 lattice structure as a result of the formation of mixed oxide phase, which in turn is in agreement with the results obtained from XRD.

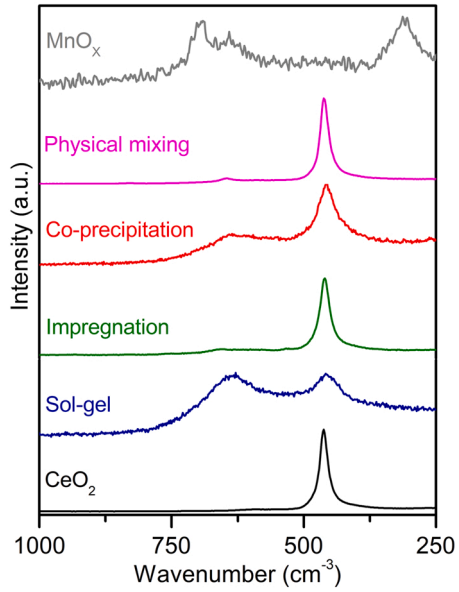

Fig. 2. Raman spectra of MnO_X-CeO_2 samples prepared by different methods.

Moreover, Raman spectra of the samples prepared by co-precipitation and sol-gel exhibit a broad band in the 700–600 cm^{-1} wavenumber region. This band is probably composed by two contributions: one associated to manganese oxide (it has been previously observed in the spectrum for pure manganese oxide), and other associated to structural defects of fluorite phase, i.e., oxygen vacancies, which are reported in the literature around 600 cm^{-1} [36]. Focusing on oxygen vacancies, they appear as a compensation of the negative charge produced by the incorporation to a lattice structure of a doping cation with different nature and oxidation state (in this specific case, the Mn^{n+} incorporation to CeO_2 lattice structure) [32]. Therefore, the appearance of oxygen vacancies is another evidence of the formation of the mixed oxide phase.

Since oxygen vacancies are linked to structural defects, the size of fluorite crystal domains will be affected, as it was previously observed by XRD. This fact could be also corroborated following the FWHM of the F_{2g} peaks, which is reported in Table 1. The samples prepared by mechanical mixing and impregnation have a similar FWHM as pure cerium oxide, whereas the FWHM value for those samples prepared by co-precipitation and sol-gel is much larger. This result evidences a decrease in the size of fluorite crystal domain, but only in the samples prepared by the methods that promote a mixed oxide phase.

Textural properties of the samples were studied by N_2-physisorption. Fig. 3A shows the obtained adsorption/desorption isotherms. According to IUPAC classification, all samples exhibit type IV isotherms with H3 hysteresis loop in the relative pressure between 0.4 and 1, which are characteristics of mesoporous materials.

Calculated specific surface areas and pore volumes are reported in Table 1. The sample prepared by co-precipitation exhibits the highest specific surface area and pore volume, whereas the remaining bimetallic samples show values ranged between pure cerium oxide and manganese oxide. These results are very interesting because they show noticeable differences at the morphological level between those catalysts prepared by co-precipitation and sol-gel, despite their similar structural properties (formation of a mixed oxide phase as a consequence of the Mn incorporation into CeO_2 structure). Therefore, this fact corroborates the key role of preparation method on textural properties.

Fig. 3B shows the pore distribution of the studied catalysts. All catalysts exhibit a pore distribution characteristic of mesoporous solids, in accordance with the type of isotherm. Nonetheless, preparation methods affect pore size distribution of the samples. The catalyst prepared by mechanical mixing presents a pore size distribution which is a combination of those of the pure oxides, whereas that prepared by impregnation exhibits pores with size around 10 nm. The catalysts prepared by co-precipitation and sol-gel show a pore distribution composed by two pore sizes: one around 4 nm, which is common for both catalysts; and the other one around 25 nm (co-precipitation) or 10 nm (sol-gel). These differences in pore sizes could be related to the different morphology provided by each preparation method.

Regarding pore distribution, it is important to note there are some discrepancies in the literature about the presence of pores with size around 4 nm in mesoporous materials when the hysteresis loop is

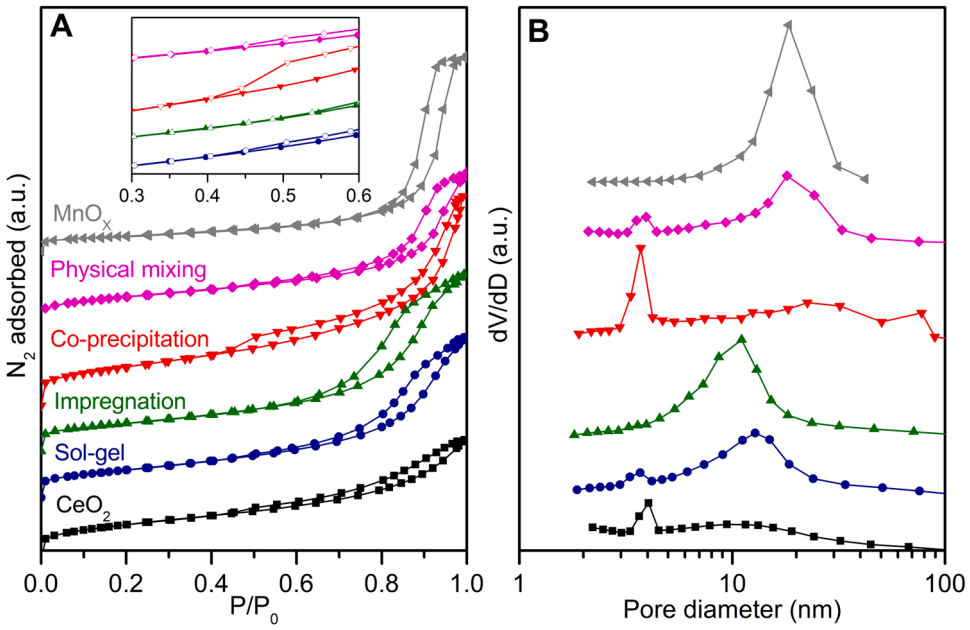

Fig. 3. A) N_2 physisorption isotherms. Inset figure: detailed view of the isotherms in the P/P_0 range 0.3–0.6. B) Pore size distribution of MnO_X-CeO_2 samples prepared by different methods.

abruptly closed in the P/P_0 range around 0.45 [37], as occurs in some of the samples here studied. This phenomenon is usually related to tensile strength effect. In this sense, the inset graph in Fig. 3 A shows a zoom of the isotherms in the P/P_0 region between 0.3 and 0.6 for the catalysts prepared by different preparation methods. Comparing the inset graph and Fig. 3B, it can be seen that the more abruptly the isotherm is closed, the more noticeable is the peak associated with pores of 4 nm. Therefore, these results suggest that pores of 4 nm are not representative of textural properties of the samples studied.

H_2-TPR was used to investigate redox properties. The reduction profiles of pure oxides, showed in Fig. 4, are quite different: pure cerium oxide exhibits two broad reduction peaks at 430 and 830 ºC related to surface and bulk cerium oxide reduction [17], respectively; whereas the reduction profile of pure manganese oxide is composed by two peaks at 290 and 420 ºC, which are associated to the reduction of Mn_2O_3 to Mn_3O_4 and Mn_3O_4 to MnO, respectively [38].

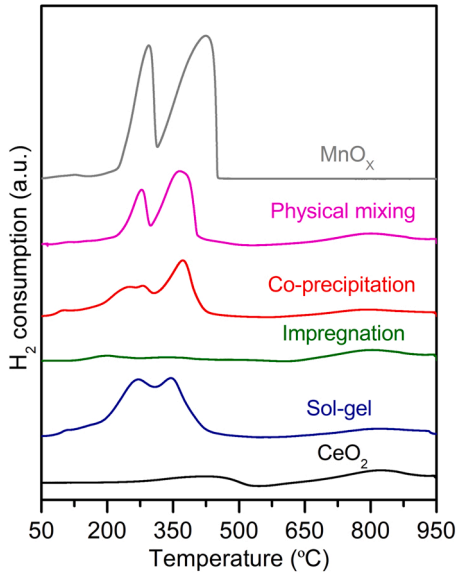

Fig. 4. H_2-TPR profiles of MnO_X-CeO_2 samples prepared by different methods.

The reduction profiles of bimetallic samples prepared by different methods exhibit two strong reduction peaks below 500 ºC, mainly associated to the reduction of Mn and, to a lesser extent, to surface Ce reduction, although the latter contribution is indistinguishable. In the case of the sample prepared by impregnation, H_2 uptake in this temperature range is very low as a consequence of its low Mn content (only surface). On the other hand, at high temperature, all the samples show the reduction peaks of bulk cerium reduction. Interestingly, Mn reduction of bimetallic samples prepared by co-precipitation and sol-gel starts at lower temperature with respect to pure oxides and the bimetallic sample prepared by mechanical mixing. This result suggests that co-precipitation and sol-gel methods lead to an improvement in the reducibility of the samples due to mixed oxide phase promotion. Mixed oxide phase has been corroborated by Raman to generate oxygen vacancies, which improves the mobility of oxygen in the lattice structure and, consequently, facilitates the reduction of the sample.

The improvement of redox properties as a result of the promotion of mixed oxide phase is not only evidenced by Mn reduction at lower temperatures, but also by the shape of reduction profiles. Thus, the catalysts prepared by co-precipitation and sol-gel show a large degree of overlap in the reduction peaks associated to Mn reduction, not observed in the sample prepared by mechanical mixing nor in the pure Mn oxide. Moreover, the samples prepared by co-precipitation and sol-gel show a small H_2 uptake around 100 ºC, which is associated in the literature to the reduction of surface Mn embedded in CeO_2 structure [39,40].

On the other hand, Table 2 shows the average oxidation state of Mn, which was estimated from the total H_2 consumption with some assumptions, such as considering that the H_2 consumption of cerium at low temperature is negligible (compared to that of Mn) and MnO is the final reduction state of Mn. The oxidation state of pure manganese oxide is very close to 3, which is in accordance with XRD results, where Mn_2O_3 was the only crystal phase identified. The bimetallic samples prepared by different methods show oxidation states of Mn between 3 and 4. Interestingly, the oxidation state of Mn is significantly higher and close to 4 in the catalysts prepared by co-precipitation and sol-gel, whereas it is close to 3 for the sample prepared by mechanical mixing. This result suggests that the promotion of mixed oxide phase favours the presence of Mn in higher oxidation state.

Since the estimation of Mn oxidation state in bimetallic samples has

Table 2
Results from H_2-TPR and NH_3-TPD analysis.

Samples	H_2 consumption (mmol H_2/g)	Mn oxidation state	Acidity		
			Total (μmol NH_3/m^2)	Weak (μmol NH_3/m^2)	Strong (μmol NH_3/m^2)
CeO_2	1.3	–	2.6	1.2	1.4
Sol-gel	4.2	3.8	3.1	1.2	1.9
Impregnation	1.4	2.8[a]	2.6	1.0	1.6
Co-precipitation	3.1	3.5	3.5	1.2	2.3
Mechanical mixing	3.6	3.3	1.2	0.5	0.7
MnO_X	6.6	3.1	5.0	2.4	2.6

[a] The estimation of Mn oxidation state for the sample prepared by Impregnation has a high contribution of error associated to the low amount of Mn loaded.

evidenced the presence of Mn^{4+} species, the assignment of the reduction peaks used for the pure manganese oxide would not be appropriate for bimetallic samples, because Mn^{4+} species would not be considered. In this sense, several works in the literature agree that Mn^{4+} reduction is indistinguishable from that of Mn^{3+}, so H_2 uptake in the strong reduction peak located at lower temperature is associated to the reduction of Mn^{4+}/Mn^{3+} to Mn_3O_4, and H_2 uptake in strong peak placed at higher temperature to the reduction of Mn_3O_4 to MnO [28,41,42].

Acid properties were evaluated by NH_3-TPD, and the NH_3 desorption profiles of the samples are shown in Fig. 5. Pure oxides exhibit two important NH_3 desorption zones: a common one around 100 ºC associated to NH_3 adsorbed over weak acid sites, and another one between 150 and 250 ºC for pure cerium oxide and at 180 ºC for pure manganese oxide, associated to NH_3 adsorbed over strong acid sites [43]. Moreover, at higher temperatures, a small NH_3 desorption is also observed between 300 and 400 ºC in both pure oxides, which suggests the presence of a small amount of even stronger acid sites. A similar result was observed by Yao and co-workers [44] after studying the NH_3 adsorption-desorption over pure CeO_2. Regarding bimetallic samples prepared by different methods, all of them exhibit the NH_3 desorption peak around 100 ºC associated to weak acid sites. However, the desorption peak associated to strong acidity is found to be shifted towards higher temperatures in the catalysts prepared by impregnation and co-precipitation. This result evidences that the presence of surface Mn and Ce favours stronger acid sites. In the case of the sample prepared by sol-gel, the peak related to strong acidity is placed at similar temperature than pure cerium oxide, although both Mn and Ce are present in the catalytic surface of this sample. This result could be related to sol-gel led to the highest distortion of fluorite phase after Mn incorporation, which caused a decrease in the crystallinity of the sample.

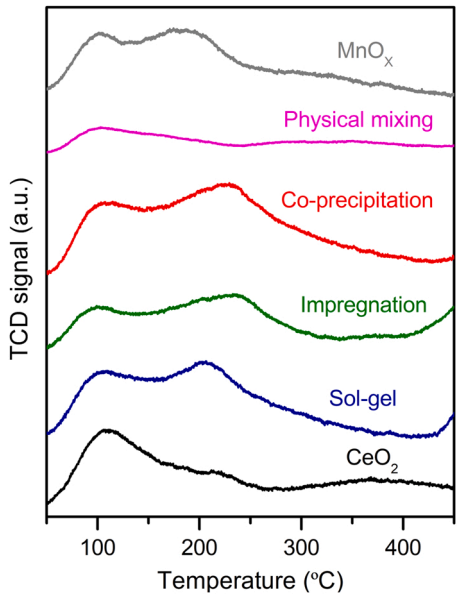

Fig. 5. NH_3-TPD profiles of MnO_X-CeO_2 samples prepared by different methods.

Table 2 summarizes total acidity of the samples per unit area. The reason for evaluating the acidity per unit area is to supress the contribution of catalytic surface area to acidity, thus analysing exclusively the effect of preparation method. Mn is the metal that contributes most to the total acidity, since pure manganese oxide is the most acidic sample. Among bimetallic samples, those prepared by co-precipitation and sol-gel are the most acidic ones. This result evidences the formation of mixed oxide phase promotes total acidity compared to the other bimetallic samples.

Table 2 also reports the contribution of preparation methods to weak and strong acidity. Weak acidity was considered to be that from NH_3 desorbed below 170 ºC, while NH_3 desorption above that temperature was related to strong acidity. Interestingly, the contribution of strong acidity to weak acidity is higher for bimetallic samples (especially for those prepared by impregnation, co-precipitation and sol-gel) than for pure oxides. This fact denotes a promotion of the strong acidity as a consequence of the presence of surface Mn and Ce, which is in accordance with the notable contribution of strong acidity in the TPD profiles of the samples prepared by co-precipitation and impregnation.

Therefore, characterization results discussed above have corroborated that the preparation methods studied in this work affect the catalytic properties differently. This effect is associated to the degree of interaction between Mn and Ce provided by each preparation method.

Co-precipitation and sol-gel methods are the ones that favoured the formation of the mixed oxide phase, through Mn incorporation to CeO_2 structure. The fact that Mn and Ce belong to the same structure, both at bulk and surface level, leads to a high interaction between both metals. The absence of mixed oxide phase in the catalysts prepared by mechanical mixing and impregnation evidences the low interaction degree between Mn and Ce at both samples. However, the results from acidity analysis, that showed a similar promotion of strong acidity in the samples prepared by impregnation and co-precipitation, suggest that the sample prepared by impregnation exhibits a similar interaction degree between the active metals at the surface level than that present in the samples prepared by co-precipitation and sol-gel.

The importance of providing a high interaction between Mn and Ce is that it produces the structural defects that promote the formation of oxygen vacancies, which improve the reducibility and favour the presence of different Mn species with high oxidation states (Mn^{4+} and Mn^{3+}). Acidity is also enhanced by preparation methods that promote a high interaction between Mn and Ce at the surface level. This property is also notoriously affected by the morphology, especially by surface area. In this sense, preparation methods have been also corroborated to affect textural properties, even when they promote similar structural properties.

In the following section, the effect of the degree of interaction between active metals (provided by the different preparation methods) on catalytic performance on the reactions under study will be addressed.

3.2. Catalytic performance

After discussing the most important points of characterization, this section aims to study the effect of preparation method on the catalytic activity in the simultaneous NO reduction and o-DCB oxidation. For this purpose, NO and o-DCB conversion as well as by-products formation will be studied.

Fig. 6 shows the NO and o-DCB conversion profiles of the samples prepared by different methods together with those corresponding to pure manganese and cerium oxides. According to Fig. 6A, pure cerium oxide has a negligible NO conversion below 200 ºC, although an increase in the temperature leads to values above 80% around 350 ºC, temperature above which NO conversion drops. On the other hand, pure manganese oxide is very active at low temperature, with NO conversion above 80% below 175 ºC. However, further temperature increase causes a small drop in NO conversion and, after an intermediate peak, a more accentuated drop can be observed at higher temperature.

Fig. 6B shows the NO conversion profiles of bimetallic samples. Similarly to pure manganese oxide sample, conversion profiles of some bimetallic catalysts show an oscillatory trend (below 250 ºC), which suggests the activation, as a function of temperature, of a set of multiple reactions that promote the consumption and formation of NO. The catalyst prepared by mechanical mixing has a different conversion profile to that calculated as the weighted sum of pure cerium and manganese oxide (showed in Fig. 6 A), although its structural and textural properties were enclosed between those observed for the pure oxides. According to this comparison, higher NO conversion is obtained with the sample prepared by mechanical mixing below 275 ºC. Thus, this result denotes that the fact of mixing both pure oxides, without the need for a preparation method that promotes a closer contact between active metals, affects to the catalytic activity.

The sample prepared by impregnation exhibits a similar conversion profile to that of the sample prepared by mechanical mixing, although with lower conversion below 300 ºC and higher above that temperature. On the other hand, the catalysts prepared by co-precipitation and sol-gel allow total NO conversion below 275 ºC. Thus, the catalysts prepared by co-precipitation and sol-gel are the most active in NO reduction, especially in the low and medium temperature range. These preparation methods were the only ones that promoted the formation of a mixed oxide phase, so their excellent activity is associated to the positive contribution of mixed oxide phase to the catalytic properties.

In the high temperature range, approximately above 275 ºC, NO conversion strongly drops in all bimetallic samples similarly to pure oxides. Then, this negative behaviour is not associated to the type of preparation method, but it is intrinsic to the reaction. In fact, a similar drop in NO conversion at high temperature is also reported for MnO_X based catalysts, either supported or doped [12,45], and other catalytic formulations such as VO_X/TiO_2 [46], Fe-ZSM5 [47] and Pt-Al_2O_3 [48]. This behaviour is associated to the prevalence of side reactions. Below, the analysis of the by-products produced in NO reduction will provide more information about this fact.

Nonetheless, although the NO conversion drop at high temperature is characteristic of NO reduction, it seems to be affected by preparation method, because in the catalysts prepared by mechanical mixing, co-precipitation and sol-gel, the drop starts around 270 ºC, whereas in the catalyst prepared by impregnation, it occurs around 330 ºC.

Regarding o-DCB oxidation, all the samples exhibit an S-shape conversion profile with two steps in which o-DCB conversion increases with temperature. Between these two steps, o-DCB conversion decays. This drop in o-DCB conversion could be caused by a deactivation of the active sites involved in the reaction at low temperature. However, the further increase in the reaction temperature favours a new increase in o-DCB conversion, which could be associated to an activation of the active sites previously deactivated or to the participation of other active sites not active at low temperature.

As for Fig. 6C, pure cerium oxide does not allow to obtain o-DCB conversions above 70% in the experimental conditions, whereas total conversion is reached with pure manganese oxide above 350 ºC. In the case of bimetallic samples, Fig. 6D, the catalyst prepared by mechanical mixing exhibit a better o-DCB conversion, especially at medium and

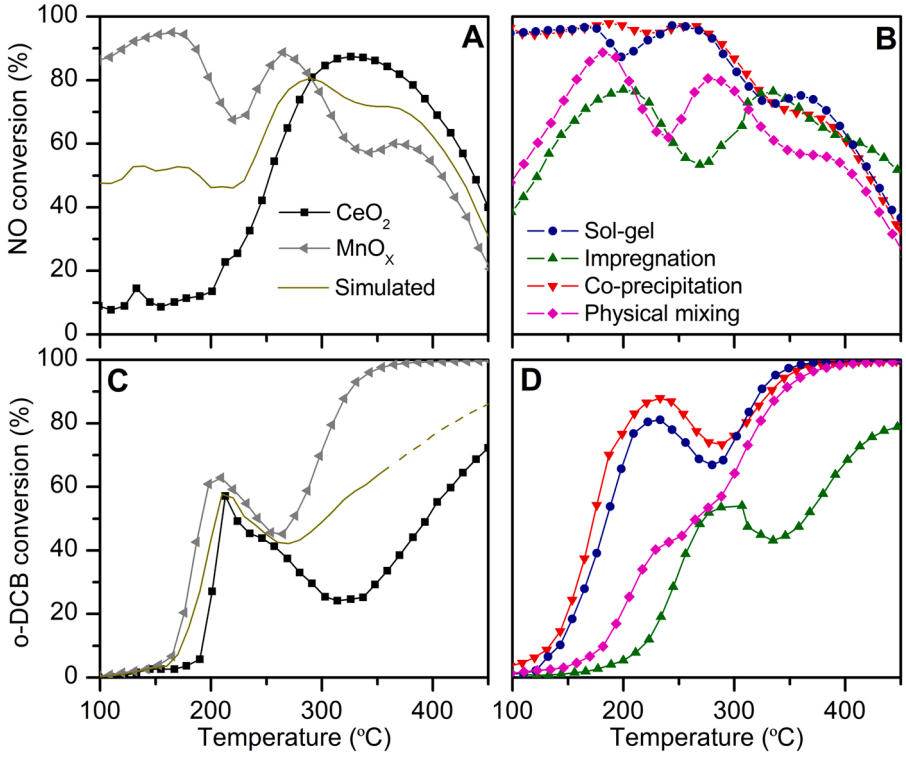

Fig. 6. NO conversion obtained with A) pure oxides and and B) bimetallic catalysts prepared by different methods. o-DCB conversion obtained with C) pure oxides and D) bimetallic catalysts prepared by different methods.

high temperature (above 275 ºC), than that calculated as the weighted sum of pure oxides (showed in Fig. 6C), which is in agreement with that observed for NO reduction. Total conversion is obtained with the sample prepared by mechanical mixing at 385 ºC. The catalyst prepared by impregnation shows the worst catalytic activity. Its conversion profile is shifted towards higher temperature and conversions above 80% are not obtained in the studied conditions.

On the other hand, the catalysts prepared by co-precipitation and sol-gel are the bimetallic samples that allow to obtain total o-DCB conversion at the lowest temperature, 350 ºC. This result evidences their higher oxidative capability, which is related to the fact that these methods promoted the formation of a mixed oxide phase that favours the oxygen mobility. This characteristic is key to perform oxidation type-reactions at lower temperature. Moreover, these samples lead to a notable increase in o-DCB conversion in the intermediate temperature range, coinciding with the first step. Thus, o-DCB conversion above 80% are obtained between 200 and 260 and 220–240 ºC for co-precipitated and sol-gel catalysts. This difference in the catalytic activity could be associated to the different textural properties.

Therefore, the results discussed above have shown that the samples prepared by co-precipitation and sol-gel exhibit the best catalytic performance in both NO reduction and o-DCB oxidation. The better catalytic activity is appreciable over the whole temperature range, although it is more noticeable at low and intermediate temperatures.

The improvement in the catalytic activity of the samples prepared by co-precipitation and sol-gel is associated to the high interaction degree between Mn and Ce, which is achieved through the formation of a mixed oxide phase. The enhancement of reaction rate and reagent adsorption through the interaction of two active metals was early proposed by Solymosi and Kiss [49] and later supported by other authors on Mn and Ce-based catalysts [15,50]. This positive effect of interaction between active metals over the catalytic activity is in agreement with the conclusion obtained in the characterization section, where important catalytic properties, such as reducibility, acidity and morphology were enhanced by the promotion of a mixed oxide phase. Thus, the interaction between Mn and Ce is postulated as a key factor for the improvement of catalytic performances.

Next, an analysis of the by-product production in each reaction will be addressed. Regarding NO reduction, N_2O and NO_2 are the main by-products identified. As can be seen in Fig. 7A, pure cerium oxide hardly produces N_2O, so the production of this by-product is mainly associated to the presence of Mn species. In fact, a notable amount of N_2O is produced with pure manganese oxide over the whole temperature range. Its production profile is maximum between 200 and 300 ºC, temperature from which the production of N_2O decreases.

In bimetallic catalysts, Figure 7B, N_2O is generated over the whole temperature range. The production profiles are quite different to those observed for pure oxides because they are composed by two peaks, which are placed at lower temperatures in the samples prepared by co-precipitation and sol-gel. According to literature [51,52], NH_3 oxidation is one of the SCR side reactions involved in N_2O production, so the shift of N_2O profile to lower temperature could be related to the higher oxidative capability of the co-precipitated and sol-gel samples, which would promote the NH_3 oxidation at lower temperature. In fact, in similar way, an improvement in the catalytic activity of o-DCB oxidation has been previously obtained with these catalysts.

As for NO_2 production, Figs. 7C and 7D show the production of this by-product takes place at temperatures above 300 ºC and its concentration increases progressively with temperature. Bimetallic samples prepared by mechanical mixing and co-precipitation exhibit the highest NO_2 production. Characterization results showed the presence of a mixed oxide phase in the sample prepared by co-precipitation, which was not formed in the samples prepared by mechanical mixing. The fact that both bimetallic samples have a similar NO_2 production, despite their notable differences at the structural level suggests that the presence of mixed oxide phase does not play a key role in the production of NO_2.

According to the previous results discussed in the analysis of catalytic activity, a strong drop in NO conversion was observed starting around 275–300 ºC (Fig. 6). This behaviour was related to the appearance of side reactions, which would consume the NH_3 needed for SCR.

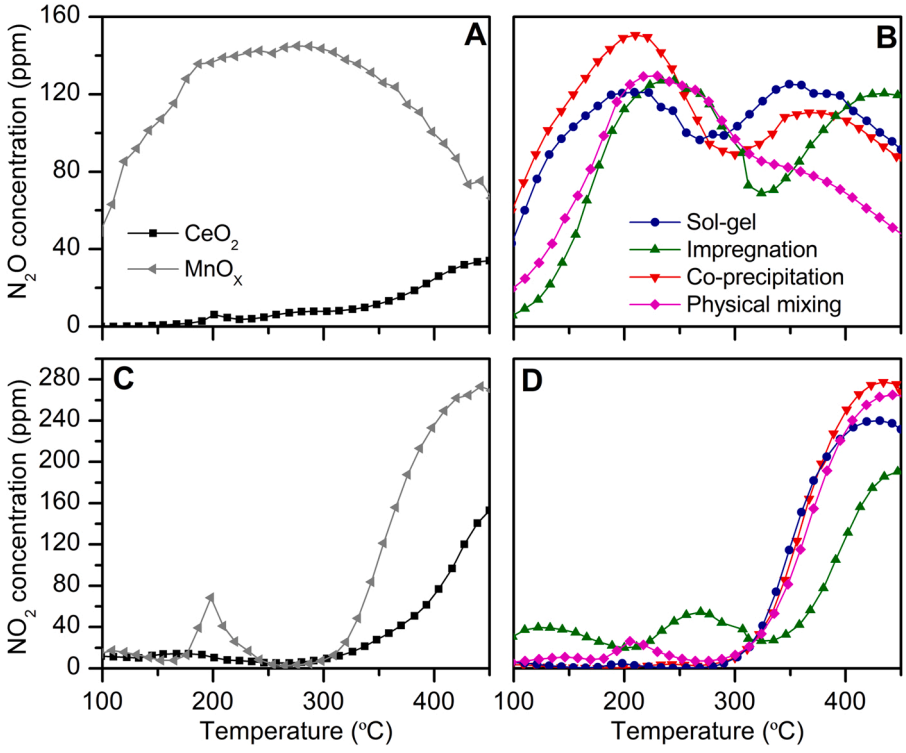

Fig. 7. N_2O generation with A) pure oxides and B) bimetallic catalysts prepared by different methods. NO_2 generation with C) pure oxides and D) bimetallic catalysts prepared by different methods.

This proposal is in agreement with the results obtained in the analysis of the by-products generated in NO reduction, since an important production of N_2O and NO_2 was found around 300 ºC.

On the other hand, the main by-products in o-DCB oxidation are CO and chlorinated organic compounds (trichlorobenzene, tetrachloromethane and tetrachloroethylene). Fig. 8 shows the selectivity towards both compounds. It is important to note that selectivity of these by-products is shown above 200 ºC, due to the low level of o-DCB conversion below this temperature.

Selectivity towards CO, Fig. 8A and B, increases gradually for pure cerium oxide with temperature, although values above 20% are not exceeded. In the case of pure manganese oxide, CO selectivity increases until reaching values around 25% between 250 and 350 ºC, temperature from which it strongly decreases. Bimetallic catalysts exhibit similar profiles to that of pure manganese oxide, although with lower values, especially the sample prepared by impregnation and also those prepared by co-precipitation and sol-gel. The lower values of CO selectivity of samples prepared by co-precipitation and sol-gel could be associated to their higher oxidative capability (as a consequence of the high oxygen mobility resulting from the presence of a solid solution), which favours a decrease in the selectivity towards those products of partial oxidation.

As for selectivity towards chlorinated organic compounds, Fig. 8C shows a different trend to that observed in the production of CO. In this case, the production of chlorinated organic compounds is higher and occurs over a wider temperature range with pure cerium oxide than with pure manganese oxide. Among bimetallic samples (Fig. 8D), the one prepared by impregnation exhibits the highest production of chlorinated organic compounds, its selectivity profile is similar to that of pure cerium oxide. The remaining bimetallic samples show a selectivity profile very similar to that of pure manganese oxide, so, similarly to the production of NO_2 in NO reduction, the presence or absence of a mixed oxide phase does not seem to affect to a great extent the production of chlorinated organic compounds.

Therefore, the promotion of a high interaction degree between Mn and Ce as a result of the formation of a mixed oxide phase, which has previously considered to play an important role in the catalytic performance, does not have a significant impact on the amount of N_2O and NO_2 produced. Nonetheless, the interaction between active metals does favor the production of N_2O at a lower temperature, due to the enhancement of the oxidative capability. The latter also promotes a lower production of CO in o-DCB oxidation, but it does not significantly affect the production of chlorinated organic compound.

4. Conclusions

Several MnO_X-CeO_2 catalysts were prepared by different methods in order to study the role they play on the Mn and Ce interaction and, also, to analyse their effect on the simultaneous NO reduction and o-DCB oxidation. Co-precipitation and sol-gel methods are the ones that promote the highest interaction degree between Mn and Ce at both surface and bulk, which is favoured by the formation of a mixed oxide phase in these samples. The interaction degree in the sample prepared by mechanical mixing is very low, whereas in the impregnated sample it is only at a surface level.

The promotion of Mn and Ce interaction is important for the catalytic activity, since those catalysts with the presence of mixed oxide phase are the most active ones over the whole temperature range, but especially at low and medium temperature, where they allow to reach total NO conversion and o-DCB conversions above 80%. This behaviour lies on mixed oxide phase promotes oxygen vacancies, which improve oxygen mobility and storage. Moreover, the interaction between active metals improves redox properties and acidity, especially strong acidity. Morphology of the sample is also affected by preparation methods, even when they lead to similar structural properties.

Regarding selectivity, N_2O and NO_2 were found as the main by-products of NO reduction. A higher interaction between active metals favours the production of N_2O at lower temperature, as a consequence of the promotion of oxidative capability. This fact also improves total o-DCB oxidation by decreasing CO production, although selectivity towards chlorinated organic compounds is not affected.

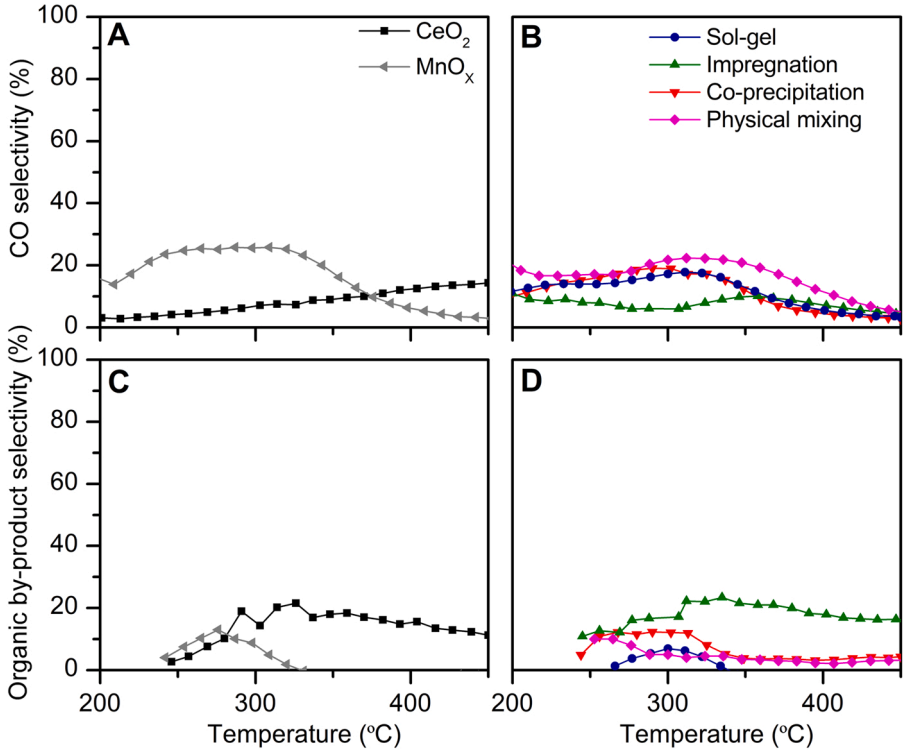

Fig. 8. CO selectivity obtained with A) pure oxides and B) bimetallic catalysts prepared by different methods. Chlorinated organic compounds obtained with C) pure oxides and D) bimetallic catalysts prepared by different methods.

CRediT authorship contribution statement

J.A. Martín-Martín:, Investigation, Conceptualization, Data curation, Writing – original draft preparation, Editing. **M.P. González-Marcos**: Supervision, Coneptualization, Reviewing **A. Aranzabal**: Supervision, Coneptualization, Writing – review & editing. **J.R. González Velasco**: Project administration, Funding acquisition.

Declaration of Competing Interest

The authors declare that they have no known competing financial interests or personal relationships that could have appeared to influence the work reported in this paper.

Data Availability

Data will be made available on request.

Acknowledgments

Authors acknowledge the financial support of MINECO (PID2019-107503RB-I00), Basque Government (IT1297-19) and The University of the Basque Country, UPV/EHU (UFI 11/39). JAMM specially thanks MINECO/FEDER (BES-2016-077849) for the PhD grant. The authors also thank technical and human support provided by SGIker of UPV/EHU and European funding (ERDF and ESF).

References

[1] Directive 2008/98/CE of the European Parliament and of the Council of 19 November 2008 on waste and repealing certain Directives (Text with EEA relevance), Official Journal of the European Union L 312 (22.11.2008), 3–30. ⟨http://data.europa.eu/eli/dir/2008/98/oj⟩.
[2] J. Lai, I.E. Wachs, A perspective on the selective catalytic reduction (SCR) of NO with NH_3 by supported V_2O_5-WO_3/TiO_2 catalysts, ACS Catal. 8 (2018) 6537–6551, https://doi.org/10.1021/acscatal.8b01357.
[3] G. Busca, L. Lietti, G. Ramis, F. Berti, Chemical and mechanistic aspects of the selective catalytic reduction of NO_X by ammonia over oxide catalysts: a review, Appl. Catal. B Environ. 18 (1998) 1–36, https://doi.org/10.1016/S0926-3373(98)00040-X.
[4] E. Finocchio, G. Busca, M. Notaro, A review of catalytic processes for the destruction of PCDD and PCDF from waste gases, Appl. Catal. B Environ. 62 (2006) 12–20, https://doi.org/10.1016/j.apcatb.2005.06.010.
[5] C. Du, S. Lu, Q. Wang, A.G. Buekens, M. Ni, D.P. Debecker, A review on catalytic oxidation of chloroaromatic from flue gas, Chem. Eng. J. 334 (2018) 519–544, https://doi.org/10.1016/j.cej.2017.09.018.
[6] M. Goemans, P. Clarysse, J. Joannès, P. De Clercq, S. Lenaerts, K. Matthys, K. Boels, Catalytic NO_x reduction with simultaneous dioxin and furan oxidation, Chemosphere 54 (2004) 1357–1365, https://doi.org/10.1016/S0045-6535(03)00255-8.
[7] X. Liu, J. Wang, X. Wang, T. Zhu, Simultaneous removal of PCDD/Fs and NO_X from the flue gas of a municipal solid waste incinerator with a pilot plant, Chemosphere 133 (2015) 90–96, https://doi.org/10.1016/j.chemosphere.2015.04.009.
[8] K. Sam-Cwan, J.S. Hwan, J. Il-Rok, K. Ki-Hun, K. Myung-Hee, K. Jae-Hyung, Y. Jun-Heung, K. Seung-Jin, Y. Jae-Cheon, J. Dong-Hee, Removal efficiencies of PCDDs/PCDFs by air pollution control devices in municipal solid waste incinerators, Chemosphere 43 (2001) 773–776, https://doi.org/10.1016/S0045-6535(00)00432-X.
[9] G. Cusano, S. Roudier, F. Neuwahl, J. Gómez-Benavides, S. Holbrook, Best Available Techniques (BAT) Reference Document for Waste Incineration, Industrial Emissions Directive 2010/75/EU (Integrated Pollution Prevention and Control), European Commission Jt. Res. Cent., Publ. Off. 2020.⟨https://data.europa.eu/doi/10.2760/761437⟩.
[10] J. Li, H. Chang, L. Ma, J. Hao, R.T. Yang, Low-temperature selective catalytic reduction of NO_x with NH_3 over metal oxide and zeolite catalysts. A review, Catal. Today 175 (2011) 147–156, https://doi.org/10.1016/j.cattod.2011.03.034.
[11] C. Liu, J. Shi, C. Gao, C. Niu, Manganese oxide-based catalysts for low-temperature selective catalytic reduction of NOx with NH3: a review, Appl. Catal. A Gen. 522 (2016) 54–69, https://doi.org/10.1016/j.apcata.2016.04.023.
[12] S. Yang, C. Wang, J. Li, N. Yan, L. Ma, H. Chang, Low temperature selective catalytic reduction of NO with NH_3 over Mn-Fe spinel: Performance, mechanism and kinetic study, Appl. Catal. B Environ. 110 (2011) 71–80, https://doi.org/10.1016/j.apcatb.2011.08.027.
[13] C. Zhang, T. Chen, H. Liu, D. Chen, B. Xu, C. Qing, Low temperature SCR reaction over nano-structured Fe-Mn oxides: characterization, performance, and kinetic study, Appl. Surf. Sci. 457 (2018) 1116–1125, https://doi.org/10.1016/j.apsusc.2018.07.019.
[14] M. Kang, E.D. Park, J.M. Kim, J.E. Yie, Cu-Mn mixed oxides for low temperature NO reduction with NH_3, Catal. Today 111 (2006) 236–241, https://doi.org/10.1016/j.cattod.2005.10.032.
[15] G. Qi, R.T. Yang, R. Chang, MnO_x-CeO_2 mixed oxides prepared by co-precipitation for selective catalytic reduction of NO with NH_3 at low temperatures, Appl. Catal. B Environ. 51 (2004) 93–106, https://doi.org/10.1016/j.apcatb.2004.01.023.
[16] S. Yang, Y. Liao, S. Xiong, F. Qi, H. Dang, X. Xiao, J. Li, N_2 selectivity of NO reduction by NH_3 over MnO_x-CeO_2: Mechanism and key factors, J. Phys. Chem. C 118 (2014) 21500–21508, https://doi.org/10.1021/jp5062489.
[17] Z. Liu, Y. Yi, S. Zhang, T. Zhu, J. Zhu, J. Wang, Selective catalytic reduction of NO_x with NH_3 over Mn-Ce mixed oxide catalyst at low temperatures, Catal. Today 216 (2013) 76–81, https://doi.org/10.1016/j.cattod.2013.06.009.
[18] Y. Shi, X. Tang, H. Yi, F. Gao, S. Zhao, J. Wang, K. Yang, R. Zhang, Controlled synthesis of spinel-type mesoporous Mn-Co rods for SCR of NO_x with NH_3 at low temperature, Ind. Eng. Chem. Res. 58 (2019) 3606–3617, https://doi.org/10.1021/acs.iecr.8b05223.
[19] F. Gao, X. Tang, H. Yi, S. Zhao, J. Wang, Y. Shi, X. Meng, Novel Co– or Ni–Mn binary oxide catalysts with hydroxyl groups for NH_3 –SCR of NO_x at low temperature, Appl. Surf. Sci. 443 (2018) 103–113, https://doi.org/10.1016/j.apsusc.2018.02.151.
[20] A. Grossale, I. Nova, E. Tronconi, D. Chatterjee, M. Weibel, The chemistry of the NO/NO_2-NH_3 "fast" SCR reaction over Fe-ZSM5 investigated by transient reaction analysis, J. Catal. 256 (2008) 312–322, https://doi.org/10.1016/j.jcat.2008.03.027.
[21] K. Qi, J. Xie, Z. Zhang, D. Fang, D. Han, X. Liu, P. Gong, F. Li, F. He, Facile large-scale synthesis of Ce–Mn composites by redox-precipitation and its superior low-temperature performance for NO removal, Powder Technol. 338 (2018) 774–782, https://doi.org/10.1016/j.powtec.2018.07.073.
[22] Y. Liu, M. Luo, Z. Wei, Q. Xin, P. Ying, C. Li, Catalytic oxidation of chlorobenzene on supported manganese oxide catalysts, Appl. Catal. B Environ. 29 (2001) 61–67, https://doi.org/10.1016/S0926-3373(00)00193-4.
[23] W. Tian, X. Fan, H. Yang, X. Zhang, Preparation of MnO_x/TiO_2 composites and their properties for catalytic oxidation of chlorobenzene, J. Hazard. Mater. 177 (2010) 887–891, https://doi.org/10.1016/j.jhazmat.2009.12.116.
[24] M.R. Morales, B.P. Barbero, L.E. Cadús, Total oxidation of ethanol and propane over Mn-Cu mixed oxide catalysts, Appl. Catal. B Environ. 67 (2006) 229–236, https://doi.org/10.1016/j.apcatb.2006.05.006.
[25] W. Tang, X. Wu, S. Li, W. Li, Y. Chen, Porous Mn-Co mixed oxide nanorod as a novel catalyst with enhanced catalytic activity for removal of VOCs, Catal. Commun. 56 (2014) 134–138, https://doi.org/10.1016/j.catcom.2014.07.023.
[26] D. Delimaris, T. Ioannides, VOC oxidation over MnO_x-CeO_2 catalysts prepared by a combustion method, Appl. Catal. B Environ. 84 (2008) 303–312, https://doi.org/10.1016/j.apcatb.2008.04.006.
[27] G. Picasso, M. Gutiérrez, M.P. Pina, J. Herguido, Preparation and characterization of Ce-Zr and Ce-Mn based oxides for n-hexane combustion: application to catalytic membrane reactors, Chem. Eng. J. 126 (2007) 119–130, https://doi.org/10.1016/j.cej.2006.09.005.
[28] H. Li, G. Lu, Q. Dai, Y. Wang, Y. Guo, Y. Guo, Efficient low-temperature catalytic combustion of trichloroethylene over flower-like mesoporous Mn-doped CeO_2 microspheres, Appl. Catal. B Environ. 102 (2011) 475–483, https://doi.org/10.1016/j.apcatb.2010.12.029.
[29] X. Wang, L. Ran, Y. Dai, Y. Lu, Q. Dai, Removal of Cl adsorbed on Mn-Ce-La solid solution catalysts during CVOC combustion, J. Colloid Interface Sci. 426 (2014) 324–332, https://doi.org/10.1016/j.jcis.2013.10.007.
[30] J.A. Martín-Martín, J. Sánchez-Robles, M.P. González-Marcos, A. Aranzabal, J. R. González-Velasco, Effect of preparation procedure and composition of catalysts based on Mn and Ce oxides in the simultaneous removal of NO_X and o-DCB, J. Mol. Catal. 495 (2020), https://doi.org/10.1016/j.mcat.2020.111152.
[31] B. Shen, X. Zhang, H. Ma, Y. Yao, T. Liu, A comparative study of Mn/CeO_2, Mn/ZrO_2 and Mn/Ce-ZrO_2 for low temperature selective catalytic reduction of NO with NH_3 in the presence of SO_2 and H_2O, J. Environ. Sci. 25 (2013) 791–800, https://doi.org/10.1016/S1001-0742(12)60109-0.
[32] S. Ramana, B.G. Rao, P. Venkataswamy, A. Rangaswamy, B.M. Reddy, Nanostructured Mn-doped ceria solid solutions for efficient oxidation of vanillyl alcohol, J. Mol. Catal. A Chem. 415 (2016) 113–121, https://doi.org/10.1016/j.molcata.2016.01.028.
[33] T. Rajkumar, A. Sápi, M. Ábel, J. Kiss, I. Szenti, K. Baán, J.F. Gómez-Pérez, Á. Kukovecz, Z. Kónya, Surface engineering of CeO_2 catalysts: differences between solid solution based and interfacially designed $Ce_{1-x}M_xO_2$ and MO/CeO_2 (M = Zn, Mn) in CO_2 hydrogenation reaction, Catal. Lett. 151 (2021) 3477–3491, https://doi.org/10.1007/s10562-021-03591-y.
[34] X. Du, D. Zhang, L. Shi, R. Gao, J. Zhang, Morphology dependence of catalytic properties of Ni/CeO_2 nanostructures for carbon dioxide reforming of methane, J. Phys. Chem. C 116 (2012) 10009–10016, https://doi.org/10.1021/jp300543r.
[35] C.M. Julien, M. Massot, C. Poinsignon, Lattice vibrations of manganese oxides: Part I. Periodic structures, Spectrochim. Acta A 60 (2004) 689–700, https://doi.org/10.1016/S1386-1425(03)00279-8.
[36] P. Venkataswamy, D. Jampaiah, C.U. Aniz, B.M. Reddy, Investigation of physicochemical properties and catalytic activity of nanostructured $Ce_{0.7}M_{0.3}O_{2-d}$ (M = Mn, Fe, Co) solid solutions for CO oxidation, J. Chem. Sci. 127 (2015) 1347–1360, https://doi.org/10.1007/s12039-015-0897-8.
[37] J.C. Groen, L.A.A. Peffer, J. Pérez-Ramírez, Pore size determination in modified micro- and mesoporous materials. Pitfalls and limitations in gas adsorption data analysis, Microporous Mesoporous Mater. 60 (2003) 1–17, https://doi.org/10.1016/S1387-1811(03)00339-1.

[38] E.R. Stobbe, B.A. De Boer, J.W. Geus, The reduction and oxidation behaviour of manganese oxides, Catal. Today 47 (1999) 161–167, https://doi.org/10.1016/S0920-5861(98)00296-X.
[39] W. Xingyi, K. Qian, L. Dao, Catalytic combustion of chlorobenzene over MnO_x-CeO_2 mixed oxide catalysts, Appl. Catal. B Environ. 86 (2009) 166–175, https://doi.org/10.1016/j.apcatb.2008.08.009.
[40] H. Chen, A. Sayari, A. Adnot, F. Larachi, Composition-activity effects of Mn-Ce-O composites on phenol catalytic wet oxidation, Appl. Catal. B Environ. 32 (2001) 195–204, https://doi.org/10.1016/S0926-3373(01)00136-9.
[41] Q. Shen, L. Zhang, N. Sun, H. Wang, L. Zhong, C. He, W. Wei, Y. Sun, Hollow MnO_x-CeO_2 mixed oxides as highly efficient catalysts in NO oxidation, Chem. Eng. J. 322 (2017) 46–55, https://doi.org/10.1016/j.cej.2017.02.148.
[42] Z. Wu, N. Tang, L. Xiao, Y. Liu, H. Wang, MnO_x/TiO_2 composite nanoxides synthesized by deposition-precipitation method as a superior catalyst for NO oxidation, J. Colloid Interface Sci. 352 (2010) 143–148, https://doi.org/10.1016/j.jcis.2010.08.031.
[43] S. Ren, J. Yang, T. Zhang, L. Jiang, H. Long, F. Guo, M. Kong, Role of cerium in improving NO reduction with NH_3 over Mn–Ce/ASC catalyst in low-temperature flue gas, Chem. Eng. Res. Des. 133 (2018) 1–10, https://doi.org/10.1016/j.cherd.2018.02.041.
[44] X. Yao, K. Ma, W. Zou, S. He, J. An, F. Yang, L. Dong, Influence of preparation methods on the physicochemical properties and catalytic performance of MnO_x-CeO_2 catalysts for NH_3-SCR at low temperature, Chin. J. Catal. 38 (2017) 146–159, https://doi.org/10.1016/S1872-2067(16)62572-X.
[45] C. Yu, B. Huang, L. Dong, F. Chen, X. Liu, In situ FT-IR study of highly dispersed MnO_x/SAPO-34 catalyst for low-temperature selective catalytic reduction of NO_x by NH_3, Catal. Today 281 (2017) 610–620, https://doi.org/10.1016/j.cattod.2016.06.025.
[46] M. Gallastegi-Villa, A. Aranzabal, Z. Boukha, J.A. González-Marcos, J.R. González-Velasco, M.V. Martínez-Huerta, M.A. Bañares, Role of surface vanadium oxide coverage support on titania for the simultaneous removal of o-dichlorobenzene and NO_x from waste incinerator flue gas, Catal. Today 254 (2015) 2–11, https://doi.org/10.1016/j.cattod.2015.02.029.
[47] R.Q. Long, R.T. Yang, Superior Fe-ZSM-5 catalyst for selective catalytic reduction of nitric oxide by ammonia, J. Am. Chem. Soc. 121 (1999) 5595–5596, https://doi.org/10.1021/ja9842262.
[48] J.H. Baik, S.D. Yim, I.- Nam, Y.S. Mok, J.- Lee, B.K. Cho, S.H. Oh, Control of NO_x emissions from diesel engine by selective catalytic reduction (SCR) with urea, Top. Catal. 31 (2004) 37–42, https://doi.org/10.1023/b:toca.0000029725.88068.97.
[49] F. Solymosi, J. Kiss, Adsorption and reduction of NO on tin(IV) oxide doped with chromium(III) oxide, J. Catal. 54 (1978) 42–51, https://doi.org/10.1016/0021-9517(78)90025-8.
[50] S. Zhang, B. Zhang, B. Liu, S. Sun, A review of Mn-containing oxide catalysts for low temperature selective catalytic reduction of NO_X with NH_3: Reaction mechanism and catalyst deactivation, RSC Adv. 7 (2017) 26226–26242, https://doi.org/10.1039/c7ra03387g.
[51] L.J. Alemany, L. Lietti, N. Ferlazzo, P. Forzatti, G. Busca, E. Giamello, F. Bregani, Reactivity and physicochemical characterization of V_2O_5-WO_3/TiO_2 De-NOx catalysts, J. Catal. 155 (1995) 117–130, https://doi.org/10.1006/jcat.1995.1193.
[52] S. Xiong, X. Xiao, Y. Liao, H. Dang, W. Shan, S. Yang, Global kinetic study of NO reduction by NH_3 over V_2O_5-WO_3/TiO_2: relationship between the SCR performance and the key factors, Ind. Eng. Chem. Res. 54 (2015) 11011–11023, https://doi.org/10.1021/acs.iecr.5b03044.